



HAL
open science

Modelling the growth stress in tree branches: eccentric growth vs. reaction wood

Arnoul van Rooij, Eric Badel, Jean-François Barczi, Yves Caraglio, Tancrede Almeras, Joseph Gril

► **To cite this version:**

Arnoul van Rooij, Eric Badel, Jean-François Barczi, Yves Caraglio, Tancrede Almeras, et al.. Modelling the growth stress in tree branches: eccentric growth vs. reaction wood. Peer Community Journal, 2023, 3, pp.e78. 10.24072/pcjournal.308 . hal-03748026v5

HAL Id: hal-03748026

<https://hal.science/hal-03748026v5>

Submitted on 7 Apr 2023 (v5), last revised 21 Nov 2023 (v6)

HAL is a multi-disciplinary open access archive for the deposit and dissemination of scientific research documents, whether they are published or not. The documents may come from teaching and research institutions in France or abroad, or from public or private research centers.

L'archive ouverte pluridisciplinaire **HAL**, est destinée au dépôt et à la diffusion de documents scientifiques de niveau recherche, publiés ou non, émanant des établissements d'enseignement et de recherche français ou étrangers, des laboratoires publics ou privés.

Modelling the growth stress in tree branches: eccentric growth *vs.* reaction wood

A. Van Rooij^{1,2}, E. Badel², J.F. Barczi³, Y. Caraglio³, T. Alméras⁴ and J. Gril^{1,2}

1. Université Clermont-Auvergne, CNRS, Institut Pascal, F-63000, Clermont-Ferrand, France

2. Université Clermont-Auvergne, INRAE, PIAF, F-63000, Clermont-Ferrand, France

3. CIRAD, UMR AMAP, F-34398 Montpellier, France.

AMAP, Univ Montpellier, CIRAD, CNRS, INRAE, IRD, Montpellier, France.

4. LMGC, CNRS, Université of Montpellier, Montpellier, France

Abstract

This work aims to model the mechanical processes used by tree branches to control their posture despite their increasing weight loading. The two known options for a branch to maintain its orientation are the asymmetry of maturation stress, including reaction wood formation, and eccentric radial growth. Both options can be observed in nature and influence the stress distribution developed in the branch each year. This so-called "growth stress" reflects the mechanical state of the branch. In this work, a growth stress model was developed at the cross-section level in order to quantify and study the bio-mechanical impact of each process. For illustration, this model was applied to branches of two 50-year-old trees, one softwood *Pinus pinaster* and one hardwood *Prunus avium* (wild cherry tree), both simulated with the AmapSim discrete element software. For the wild cherry tree, the computed outputs highlighted that the eccentricity of radial growth seems to be as efficient as the formation of reaction wood to maintain the postural control despite the increasing gravity. For the pine tree, eccentric radial growth appears to be less efficient than the formation of reaction wood. But although it does not necessarily act as a relevant lever for postural control, it greatly modifies the profile pattern of mechanical stress and could provide mechanical safety of the branch. This work opens experimental perspectives to understand the biomechanical processes involved in the formation of branches and their mechanical safety.

25 Abbreviations and notations (in order of occurrence)

NW, TW, CW	Normal Wood, Tension Wood, Compression Wood
(x, y, z)	Local reference coordinates associated with the section
O	Centre of the section
r, R	Radial polar coordinate and Radii of the cross section (m)
$e(R), \bar{e}(R)$	Eccentricity at the stem radius R, integrated eccentricity up to $r = R$
(x', y', z')	Local reference coordinates associated with the section, centred on the pith
σ	Stress (MPa)
σ_0	Induced maturation stress (Mpa)
S	Cross section area (m^2)
N, M	Loads (N): normal force parallel to z' and bending moment around y'
E	Module of elasticity in L direction (GPa): MOE
μ	Induced maturation strain
ϵ, a, b	Strain, at the center, local curvature
K_i	Structural stiffness of the cross-section
F_i	External coefficients (maturation and load)
θ	Circumferential position in section (rad)
$\sigma_0(\theta)$	Maturation strain in the new ring at circumferential position θ
α	Mean maturation stress in the new ring
β	Differential stress in the new ring
$R_{x'y'}$	Radius of the cross section at the instant of appearance of the point (x', y')
$\lambda_N, \lambda_M, \nu_M, \nu_N$	Load power law: allometric coefficient
λ_b, ν_b	Change of curvature power law: allometric coefficient
$\sigma_{NW}, \sigma_{TW}, \sigma_{CW}$	Maturation stress in the normal wood, tension wood and compression wood
$\mu_{NW}, \mu_{TW}, \mu_{CW}$	Maturation strain in the normal wood, tension wood and compression wood
\vec{N}_n, \vec{M}_n	Loads of growth unit n: normal force and bending moment around y
N_z, M_x, M_y, M_z	Loads of growth unit n: projection of \vec{N}_n on \vec{z} and bending moment \vec{M}_n around $\vec{x}, \vec{y}, \vec{z}$
m_n	Mass of the growth unit n (kg)
g	Gravity constant: $g = 9.8 \text{ m.s}^{-2}$
G_n	Centre of gravity of the growth unit n
E_d, E_g	Air-dry, green MOE
ρ	Density
μstrain	$1/10^6$
D_n, D_{n+1}	First and second diameter the growth unit n
D_f	Deflection of a growth unit
L_n	Length of the growth unit n

28 Introduction

29 From a mechanical point of view, wood in trees fulfils three major functions: construction of the tree
30 structure, postural control of trunk and branches and breaking resistance to external stimuli [Thibaut
31 (2019)]. These three functions are provided by the way wood cells differentiate and accumulate during
32 the wood formation process. Each axis of a tree can be considered as an inclined beam, consisting of
33 a succession of conical growth units [Barthélémy and Caraglio (2007)]. It is built in two steps: first,
34 primary growth resulting in new growth units that increase the length of the initial axis; and secondary
35 growth resulting in thickening of already existing units by addition of annual rings. These two interactive
36 and additional processes lead to a specific pattern of mechanical stress, called 'growth stress', which can
37 be analysed as the superposition of support stress and maturation stress [Archer (1976); Fournier et al.

(1991a)]. The support stress results from the continuous increase of the weight supported by the axis over the years. It reaches maximal levels close to the stem and vanishes near stem periphery, where the recently formed wood contributes to the support of recently produced biomass only. Maturation stress is set up at the end of the cell-wall maturation process, when molecular components such as lignin polymerise, generating growth forces by small dilatation or contraction restrained by the rigidity of the previously formed wood cells [Alméras and Clair (2016)]. An evaluation of the maturation stress can be obtained by measuring the strain associated to stress release at stem periphery, where no support stress is present [Nicholson (1971); Yoshida and Okuyama: (2002); Yang et al. (2005)]. The circumferential heterogeneity of this peripheral stress is needed to regulate stem curvature. In most cases, a tensile maturation stress is produced in the newly formed 'normal wood'. But observations on inclined trunks [Alméras et al. (2005); Coutand et al. (2007); Thibaut and Gril (2021)], seedlings [Hung et al. (2016)] and branches [Fisher and Stevenson (1981); Huang et al. (2010); Tsai et al. (2012); Hung et al. (2017)] have evidenced a clear difference between hardwood and softwood. Hardwoods produce 'tension wood', inducing a much higher tensile stress on one side, while for softwood, a compressive stress is induced in 'compression wood'. The first pulls, the second pushes. In the most usual case of inclined stems restoring their vertical orientation, tension wood is formed on the upper side while compression wood is formed on the lower side of the trunk. But other situations can be encountered depending on the biomechanical requirements of the tree [Wang et al. (2009b)]. In addition to their participation in the postural control of tree stems, these two types of so-called 'reaction wood' are characterised by specific anatomical pattern (not discussed here) and specific physical and mechanical properties.

As an alternative to complex experimental approaches, growth stress modelling plays an important role in the understanding of the phenomena involved in the orientation process of a stem. The history of biomechanical models began with Kübler (1959) who proposed an analytical formulation of growth stress for a perfect cylinder made of a homogeneous and transversally isotropic wood. Later, Archer and Byrnes (1974) took into account an asymmetry of the maturation stress, and Fournier et al. (1991a,b) proposed a semi-incremental version of these models, allowing to take into account a potential gradient of mechanical parameters (stiffness, maturation).

By associating their previous model to the loading induced by the tree weight, Fournier et al. (1994) made the connection between growth stress and stem orientation. This model has been adopted and developed by several authors in order to study the orientation process of stems. Yamamoto et al. (2002) added a primary shoot and returned to curvature calculations. Alméras and Fournier (2009) introduced the notion of gravitropic performance (capacity of the tree to correct the bending moment induced by its weight) and proposed criteria of long-term stability. Huang et al. (2005) and Alméras et al. (2005) improved the model by introducing a secondary growth asymmetry and its resulting pith eccentricity, as well as stiffness heterogeneity, allowing to quantify the effectiveness of eccentricity, maturation, stiffness gradient and initial radius in the curvature regulation process. They highlighted that the main factor in the gravitropic process is the spatial distribution of the maturation stress. Still in line with Fournier's 1994 model, Alméras et al. (2018) recently developed analytical models of longitudinal growth stress, taking into account different configurations, like eccentricity or maturation gradient, and evolution laws, like evolution of stiffness per additional layer. Finally, based on the same philosophy as established by Kübler, tree-scale and finite-element models have emerged [Fourcaud et al. (2003); Ancelin et al. (2004)].

Huang et al. (2010)'s model has been used to understand how eccentric growth and reaction wood are involved in branch orientation [Wang et al. (2009a); Huang et al. (2010); Tsai et al. (2012); Hung et al. (2017)], but all these studies were based on the current state of the branch, without consideration of the previous history: although some of them quantified the roles of maturation and eccentricity in the regulation of curvature, none did evaluate their capacity to ensure a given growth scenario.

Unlike trunks, which usually seek verticality, after the first stages of growth, branches tend to grow in a stationary way at a fixed angle to the vertical. Therefore, in this framework, we focus on understanding

87 how branches can control their orientation, through the study of two growth parameters: eccentric growth
88 and compression wood. The aim is to check by calculation what option is mechanically possible and safe
89 for the branch. For this purpose, we developed a semi-incremental biomechanical model of growth stress
90 at the cross section level that takes into account the eccentricity and maturation gradients during the
91 construction of branches. Using the digital models of a softwood (*Pinus pinaster* Aiton) and a hardwood
92 (*Prunus avium* L), the impact of each of these two growth parameters on the stress state was evaluated.

93 Material and methods

94 Numerical model

95 General hypotheses

96 The problem was set in the framework of the beam theory. From a geometrical point of view, branches
97 generally show profiles that suit to this type of analytical framework: a slender shape and no important
98 diameter variations. The shape effects due to twigs and other local biological phenomena (cavity, nodes,
99 etc.) were neglected. The same set of hypotheses as in Alméras et al. (2018) was adopted. In this study,
100 we focused on the behaviour in the longitudinal direction (parallel to the main axis). Horizontal bending
101 and torsion loads were not considered. Only the vertical bending moment (caused by the weight) was
102 considered; these hypotheses on the loading modes are discussed later.

103 Geometrical settings

104 The object of study was the cross-section of a branch, placed within a plane locally orthogonal to the pith.
105 The local reference frame of the section is $(\vec{x}, \vec{y}, \vec{z})$, with \vec{z} the longitudinal direction of the axis, and \vec{x}
106 placed in a vertical plane and facing upwards (Fig 1). The shape of the cross-section was assumed to be
107 circular at any stage of development, described by the successive depositions of wood rings. The term of
108 'ring' refers here to the volume occupied by wood cells produced by the cambium during a certain duration
109 of time, not necessarily annual: it must be taken in a numerical meaning. These rings possibly could
110 present an eccentricity resulting from asymmetry of secondary growth. Since the model only takes into
111 account vertical bending, the eccentricity was set along the x axis, as expressed by the following equation:

$$O(t) = \int_0^{R(t)} e(r)dr = \bar{e}R(t) \quad (1)$$

112 with $O(t)$ the position of the geometrical centre and $R(t)$ the radius of the section at time t , $e(r)$ the
113 eccentricity when the stem radius was r and \bar{e} the integrated eccentricity up to $r = R$. The eccentricity can
114 vary in the interval $[-1, 1]$. A zero eccentricity corresponds to a centred section, while -1 or 1 corresponds
115 to maximum eccentricity resulting from secondary growth only on the lower or the upper side of the
116 section, respectively. In the following, the position x' in the pith reference frame is needed. By calling x
117 the vertical position in the geometrical reference frame, we deduce from equation (1):

$$x = x' - \bar{e}R \quad (2)$$

118 Computation of the mechanical behaviour

119 We developed a radial incremental method. For each radial increment, the longitudinal stress was computed
120 in order to satisfy the static equilibrium of the cross section:

$$\begin{cases} \int_S \delta\sigma dS + \int_{\delta S} \sigma_0 dS = \delta N & (3a) \\ \int_S \delta\sigma x dS + \int_{\delta S} \sigma_0 x dS = -\delta M & (3b) \end{cases}$$

121 where S is the cross-section area, δS is its increment, $\delta\sigma$ is the increment of stress σ in the already formed
 122 wood, in response to the maturation stress σ_0 generated in the new wood layer. δN and δM are respectively
 123 the increment of external force N and bending moment M , that are applied on the cross-section. For
 124 illustration, the geometric situation for K rings and an increment of stem radius δR is proposed in Fig 1.

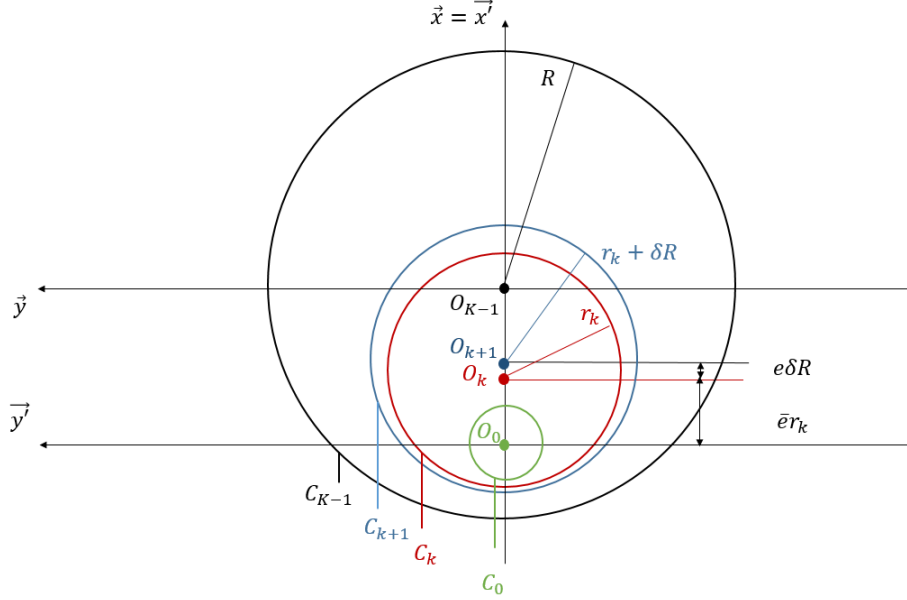


Figure 1: Geometrical representation of a section with K numerical rings and a radial increment δR between rings $(k - 1)$ and k .

125

126 The stress σ is linked to the strain ϵ by a classical pre-stressed Hooke's law:

$$\sigma = E(\epsilon - \mu) = E\epsilon + \sigma_0 \quad (4)$$

127 where E is the longitudinal Young's modulus, μ is the maturation strain and σ_0 is the maturation stress.
 128 In the context of the beam theory, the planar cross-sections remain so (Euler-Bernouilli assumption). The
 129 strain field is then described by the deformation a at the centre of the pith and the curvature b relative to
 130 the y -axis, as follows:

$$\delta\epsilon = \delta a + x\delta b \quad (5)$$

131 where $\delta\epsilon$, δa , δb are the increments of ϵ , a , b , respectively. The stress increment $\delta\sigma$, in the already formed
 132 wood, where no maturation occurs anymore, can then be deduced:

$$\delta\sigma = E\delta\epsilon = E(\delta a + x\delta b) \quad (6)$$

From these considerations, the system (3) becomes (details of the calculation are given in Appendix A):

$$\begin{cases} K_0\delta a + K_1\delta b = \delta F_0 \\ K_1\delta a + K_2\delta b = \delta F_1 \end{cases} \quad (7a)$$

$$\begin{cases} K_1\delta a + K_2\delta b = \delta F_1 \end{cases} \quad (7b)$$

133 with

$$K_0 = E\pi R^2, \quad K_1 = E\pi\bar{e}R^3, \quad K_2 = E\pi R^4 \left(\bar{e}^2 + \frac{1}{4} \right) \quad (8)$$

$$\delta F_0 = - \int_{\delta S} \sigma_0 dS + \delta N, \quad \delta F_1 = - \int_{\delta S} \sigma_0 x dS - \delta M$$

134 The calculation of the coefficients δF_0 and δF_1 depends on the formulation of the maturation stress. The
 135 maturation stress was assumed to vary circumferentially as follows:

$$\sigma_0(\theta) = \alpha + \beta \cos \theta \quad (9)$$

where the mean stress α and differential stress β were defined differently in softwood and hardwood species:

$$\left\{ \begin{array}{l} \text{Hardwood: } \alpha = \frac{\sigma_{TW} + \sigma_{NW}}{2}; \beta = \frac{\sigma_{TW} - \sigma_{NW}}{2} \end{array} \right. \quad (10a)$$

$$\left\{ \begin{array}{l} \text{Softwood: } \alpha = \frac{\sigma_{CW} + \sigma_{NW}}{2}; \beta = \frac{\sigma_{NW} - \sigma_{CW}}{2} \end{array} \right. \quad (10b)$$

σ_{TW} (resp. σ_{CW}) being the maturation stress in the tension wood (resp. compression wood), and σ_{NW} that in the opposite wood. One gets :

$$\left\{ \begin{array}{l} \delta F_0 = -\pi R (2\alpha + e\beta) \delta R + \delta N \end{array} \right. \quad (11a)$$

$$\left\{ \begin{array}{l} \delta F_1 = -\pi R^2 (3\alpha e + e^2\beta + \beta) \delta R - \delta M \end{array} \right. \quad (11b)$$

136 From equations (8), (11a) and (11b), the components of the system (7) are known. By inversion, $\delta\alpha$ and
 137 δb can be obtained according to the following equations (see details in Appendix B):

$$\left\{ \begin{array}{l} \delta a = \frac{4}{ER} \left[\left(3e\bar{e} - 2e^2 - \frac{1}{2} \right) \alpha + \left(\bar{e}e^2 - e\bar{e}^2 + \bar{e} - \frac{e}{4} \right) \beta \right] \delta R + \frac{4}{E\pi R^3} \left[\bar{e}\delta M + \left(\bar{e}^2 + \frac{1}{4} \right) R\delta N \right] \end{array} \right. \quad (12a)$$

$$\left\{ \begin{array}{l} \delta b = \frac{-4}{ER^2} \left[(3e - 2\bar{e}) \alpha + (e^2 - e\bar{e} + 1) \beta \right] \delta R - \frac{4}{E\pi R^4} (\delta M + \bar{e}R\delta N) \end{array} \right. \quad (12b)$$

138 Once δa and δb are known, the stress increment $\delta\sigma$ at any position given by (x', y') can be obtained from
 139 equation(6). The stress distribution at this position can be obtained as the sum of the initial maturation
 140 stress and all the stress increments undergone by the material point since its creation.

$$\sigma(x', y', R) = \sigma_0(x', y') + \sum_{k=k_{x'y'}}^K \delta\sigma_k \quad (13)$$

141 where $\delta R_k = r_k - r_{k-1}$ for a succession of ring radii $0 < r_0 < \dots < r_k < \dots < r_K = R$, $\delta\sigma_k$ is the
 142 corresponding increment, and $k_{x'y'}$ designates the ring containing the point.

143 Analytical formulations

144 Using equations (12b) and dividing by δR , we get the following equations when δR tends to zero :

$$\left\{ \begin{array}{l} \frac{da}{dR} = \frac{4}{ER} \left[\left(3e\bar{e} - 2e^2 - \frac{1}{2} \right) \alpha + \left(\bar{e}e^2 - e\bar{e}^2 + \bar{e} - \frac{e}{4} \right) \beta + \frac{1}{\pi R^2} \left(\bar{e} \frac{dM}{dR} + \left(\bar{e}^2 + \frac{1}{4} \right) R \frac{dN}{dR} \right) \right] \end{array} \right. \quad (14a)$$

$$\left\{ \begin{array}{l} \frac{db}{dR} = \frac{-4}{ER^2} \left[(3e - 2\bar{e}) \alpha + (e^2 - e\bar{e} + 1) \beta + \frac{1}{\pi R^2} \left(\frac{dM}{dR} + \bar{e}R \frac{dN}{dR} \right) \right] \end{array} \right. \quad (14b)$$

145 Using equation (13) and dividing again by a vanishing δR , we obtain the following equation involving the
 146 partial derivative $\partial\sigma/\partial R$:

$$\sigma(x', y', R) = \sigma_0(x', y') + \int_{R_{x'y'}}^R \frac{\partial\sigma}{\partial R}(x', R') dR' \quad (15)$$

147 where $R_{x'y'}$ is the radius of the section at the instant of appearance of the point with coordinates (x', y') .

On the other hand, the expressions of axial force $N(R)$ and bending moment $M(R)$ are required to compute the evolution of the stress distribution in the cross section. For this purpose, we assumed that both vary as a power function of the radius of the branch. This resulted in the following allometric laws:

$$\begin{cases} N = \lambda_N R^{\nu_N} & (16a) \\ M = \lambda_M R^{\nu_M} & (16b) \end{cases}$$

148 where $\lambda_{N,M}$ and $\nu_{N,M}$ are allometric coefficients. The λ -coefficients are directly proportional to the weight
149 of the branch part supported by the cross section (the branch itself and the other axes of higher orders).
150 The ν -coefficients express the kinetics of the secondary growth: a small ν refers to an early secondary
151 growth while a higher one refers to a later diameter increase.

152

The calculation of σ requires also the knowledge of the temporal variation of the curvature b . In order to simplify the analyses, we mainly studied stationary cases, i.e. we assumed that the branch maintains its orientation and remains straight. This assumption results in $\frac{db}{dR} = 0$. Physiologically, this equation expresses that the branch always compensates its weight increment at each deposition step of a new wood layer, corresponding to an additional weight. However, we can consider two cases for which the branch does not build up in a stationary way: i) the passive bending (under its own weight) case, and ii) the up-righting case (i.e. the action of maturation is stronger than the additional weight). In both cases, the resulting change in curvature has been modelled by Alm eras and Fournier (2009) and Alm eras et al. (2018). It can then be written as follows:

$$\begin{cases} \text{Up-righting:} & \frac{db}{dR} = -4 \frac{\beta}{ER^2} & (17a) \\ \text{Passive bending:} & \frac{db}{dR} = 4 \frac{\lambda_M \nu_M}{E\pi} R^{\nu_M-5} & (17b) \end{cases}$$

153 For the next computations, we used the following general law:

$$\frac{db}{dR} = \lambda_b R^{\nu_b} \quad (18)$$

154 As a remark, even if this equation bears some resemblance to (16), it does not express any notion of
155 allometry and is used here only for convenience. Combining (14),(15),(16) and (18), the total stress can
156 then be computed as:

$$\sigma^i(x', y', R) = \sigma_0^i(x', y') + S_1 \ln\left(\frac{R}{R_{x'y'}}\right) + \frac{S_2}{S_3} (R^{S_3} - R_{x'y'}^{S_3}) + \frac{S_4}{S_5} (R^{S_5} - R_{x'y'}^{S_5}) + \frac{S_6}{S_7} (R^{S_7} - R_{x'y'}^{S_7}) x' \quad (19)$$

157 where $S_1 = 4 \left[\left(3e\bar{e} - 2e^2 - \frac{1}{2} \right) \alpha + (\bar{e}e^2 - e\bar{e}^2 + \bar{e} - \frac{e}{4}) \beta \right]$ is driven by the maturation process, $S_2 =$
158 $\frac{\lambda_N \nu_N}{\pi} \left(\bar{e}^2 + \frac{1}{4} \right)$, $S_3 = \nu_N - 2$, $S_4 = \frac{4}{\pi} \lambda_M \nu_M \bar{e}$ and $S_5 = \nu_M - 3$ by the branch loading (geometric evolution
159 of the branch), $S_6 = E\lambda_b$ and $S_7 = \nu_b + 1$ by the branch orientation.

160 For each radius r , the remaining unknowns are the mean stress α , the differential stress β and the
161 eccentricity e . Equation (14b) can be rewritten as:

$$(3e - 2\bar{e}) \alpha + (e^2 - e\bar{e} + 1) \beta = \frac{-1}{\pi R^2} \left(\frac{dM}{dR} + \bar{e} R \frac{dN}{dR} \right) - E \frac{R^2}{4} \frac{db}{dR} \quad (20)$$

162 Thus by fixing two parameters, the third is directly determined. The maturation parameters α and β are
163 determined by the maturation stress σ_{NW} in normal wood and σ_{TW} or σ_{CW} in reaction wood according
164 to equation (10).

165 We considered two possible configurations for the simulations in the next section:

-
1. First, we applied a constant eccentricity (so that $\bar{e} = e$) and we fixed the stress level in the normal wood. In that case, the maturation stress of the reaction wood was given by equations (10):

$$\left\{ \begin{array}{l} \sigma_{TW} = \frac{-2}{\pi R^2(1+e)} \left(\frac{dM}{dR} + eR \frac{dN}{dR} \right) + \sigma_{NW} \left(\frac{1-e}{1+e} \right) + \lambda_b \left(\frac{ER^2}{2(1+e)} \right) R^{\nu_b} \\ \sigma_{CW} = \frac{2}{\pi R^2(1-e)} \left(\frac{dM}{dR} + eR \frac{dN}{dR} \right) + \sigma_{NW} \left(\frac{1+e}{1-e} \right) - \lambda_b \left(\frac{ER^2}{2(1-e)} \right) R^{\nu_b} \end{array} \right. \quad (21a)$$

$$\left\{ \begin{array}{l} \sigma_{TW} = \frac{-2}{\pi R^2(1+e)} \left(\frac{dM}{dR} + eR \frac{dN}{dR} \right) + \sigma_{NW} \left(\frac{1-e}{1+e} \right) + \lambda_b \left(\frac{ER^2}{2(1+e)} \right) R^{\nu_b} \\ \sigma_{CW} = \frac{2}{\pi R^2(1-e)} \left(\frac{dM}{dR} + eR \frac{dN}{dR} \right) + \sigma_{NW} \left(\frac{1+e}{1-e} \right) - \lambda_b \left(\frac{ER^2}{2(1-e)} \right) R^{\nu_b} \end{array} \right. \quad (21b)$$

- 166 2. Second, we fixed the maturation parameters and we observed how the eccentric growth could, or not,
 167 maintain the orientation of the branch. In this configuration, equation (20) became a two degrees
 168 equation in e that could be solved numerically.

169 In these two configurations, using data on the support allometries $\lambda_N, \lambda_M, \nu_M, \nu_N$, we can calculate the
 170 stress in the reaction wood and/or the eccentricity with different (λ_b, ν_b) , then deduce the growth stress
 171 profile in the section (eq. 19). In the next part, we see how the allometric coefficients can be obtained
 172 from data generated by growth model.

173 Realistic growth data

174 Tree architecture modelling

175 Numerical experiments were carried out using two reference models: a softwood, maritime pine (*P.*
 176 *pinaster*) and a hardwood, wild cherry (*P. avium*) (Fig 2). Their growth follows the architectural model
 177 of Rauh [Hallé et al. (1978)]. This implies that the branching is rhythmic, the axes are monopodial and
 178 the branches are orthotropic. These digital trees were computed with the AmapSim software [Barczi et al.
 179 (2007)]. The input of this software are architectural parameters which were provided by observations
 180 and field studies: Coudurier et al. (1993) and Heuret et al. (2006) for *P. pinaster*, Caraglio (1996) and
 181 Barthélémy et al. (2009) for *P. avium*. The choice of these species was based on the availability of
 182 temperate species in the AmapSim database. The two trees were modelled over 50 years in open-growth
 183 conditions, which did not correspond to the same ontogenic stage of development, but allowed both trees
 184 to be considered mature. In the final state, the pine (resp. cherry) was 18,2 m (resp. 14,1 m) high. The
 185 diameter at the base was 40 cm for both species. The insertion height of the first branch was 14,3 m for
 186 pine and 4,6 m for the birch. The branches of interest were the main branches; those that were directly
 187 attached to the trunk. In addition, only branches that were more than 20 years old were studied, so that
 188 they had a consistent loading history. Finally, 33 branches for the pine and 45 for the birch were selected.
 189 For each of the branch groups, the distributions of length L , radius r and insertion angle with the trunk θ
 190 are shown in Table 1.

Species	L_m (m)	r_m (m)	θ_m (°)
<i>Pinus pinaster</i>	5.3 ± 0.4	5.2 ± 0.3	70 ± 0.01
<i>Prunus avium</i>	7.9 ± 1.4	8.1 ± 0.7	80 ± 0.05

Table 1: Geometric distribution of branches of interest

193 Loading scenarii: allometric laws

194 Each tree was composed of axes organised hierarchically according to their order: 1 for the tree seed, 2
 195 for the trunk, 3 for the main branches, 4 for those attached to them, etc.. Each axis was described as a
 196 succession of growth units, which were sections of cones, identified by a number (in order of appearance),
 197 and defined by a parent number, an order, a start and end diameter, the coordinates of the centres of both
 198 initial and final sections as well as their length (Fig 3). Note that the description provided by AmapSim



Figure 2: AmapSim representation of aerial architecture of 50-years old trees. (a) *Prunus avium* and (b) *Pinus pinaster*

199 did not include the internal structure of the growth units, such as eccentricity. To avoid unnecessary
 200 complications, the coordinates of the centres were taken as those of the pith. From the model data, the
 201 moments and normal forces can be computed in each growth unit, at any time of the tree's existence.
 202 In addition to a part of its own weight, each unit is subjected to the weight of its offsprings - this term
 203 referring to any growth unit that would fall if the studied one was cut. The normal force \overrightarrow{N}_n and bending
 204 moment \overrightarrow{M}_n supported by the growth unit n can be written:

$$\overrightarrow{N}_n = \frac{1}{2}m_n\vec{g} + \sum_{\substack{k>n \\ k \text{ offspring}}} m_k\vec{g} \quad (22)$$

205

$$\overrightarrow{M}_n = \overrightarrow{G_n G'_n} \wedge \left(\frac{1}{2}m_n\vec{g} \right) + \sum_{\substack{k>n \\ k \text{ offspring}}} \overrightarrow{G_n G_k} \wedge (m_k\vec{g}) \quad (23)$$

206 where G_n is the centre of gravity of the current growth unit, G'_n is the centre of gravity of its second half.
 207 On the downstream side of G_n , G_k is the centre of gravity of an offspring of number $k > n$, m_i is the mass
 208 of growth unit i and \vec{g} is the gravity vector. Once \overrightarrow{N}_n and \overrightarrow{M}_n were computed in the absolute coordinates
 209 used for the description of the whole tree, they were projected in the local coordinates system $(\vec{x}', \vec{y}', \vec{z})$,
 210 with \vec{z} of the chosen cross section. In the following, in accordance with the development of the previous
 211 section, N_z refers to the projection of \overrightarrow{N} on \vec{z} and M_y to the projection of \overrightarrow{M} on \vec{y}' .

212 Power law regressions were performed to recover the allometric coefficients $\lambda_M, \lambda_N, \nu_N, \nu_M$. A summary
 213 of the analysis process is proposed in Fig 3.

214 For the selected branch groups, the distribution of all allometric coefficients are presented in Fig 4. In *Pinus*,
 215 there was a large variation in ν -coefficient, with ν_M varying by almost a factor 2 in the studied sample;
 216 indicating very variable secondary growth kinetics. In *Prunus*, the range of variation of the allometric
 217 power coefficients was smaller, which depicted a higher homogeneity of secondary growth kinetics. For
 218 both species, a great diversity in λ - coefficients was observed, which depicted a significant variability
 219 in the loading history. This is particularly interesting as the branches showed geometric determinants

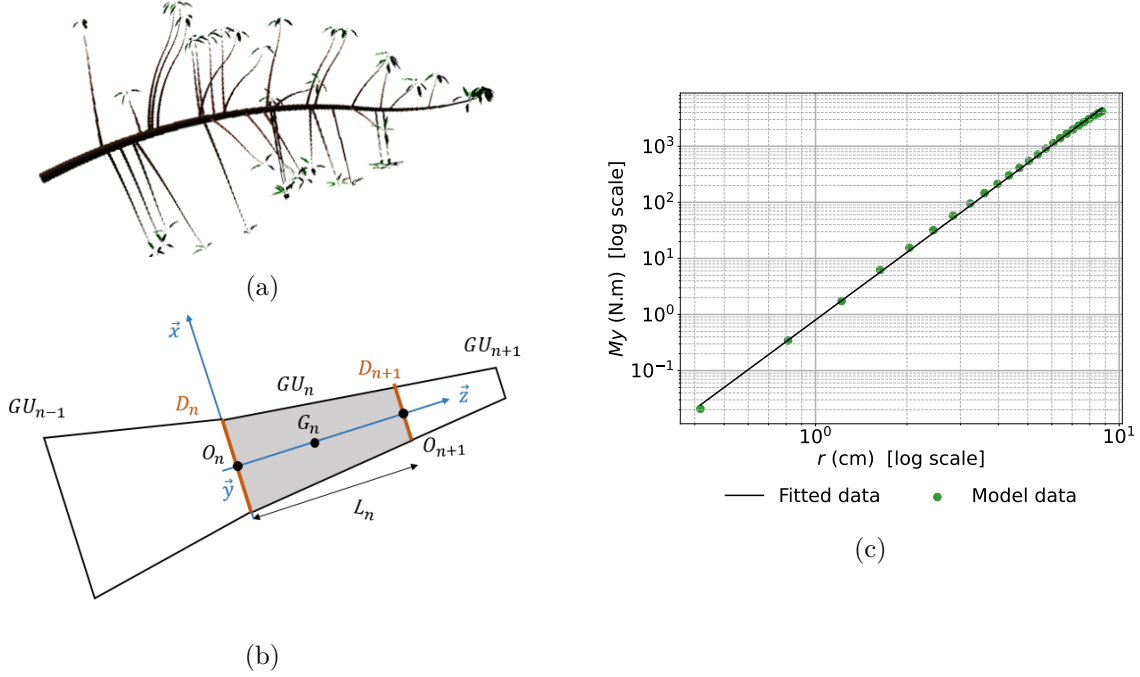


Figure 3: Illustration of the different steps of computation of the allometric law $M_y = f(r)$. First the modelled branch of *P. avium* (a) was divided into a succession of conical units (b). This allowed to compute the bending moment M . Then, the repetition of the computation each year, provided the relationship between the branch radius r and the bending moment M_y , represented in the graph (c). The fitted curve provides the final allometric law.

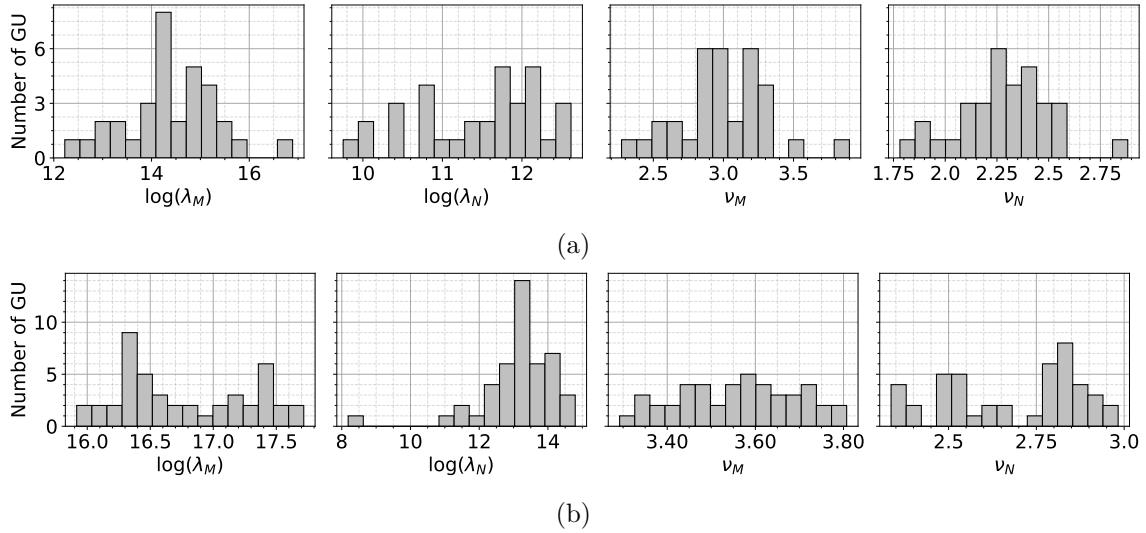


Figure 4: Statistical distribution of allometric coefficients for modelled branches: (a) *Pinus pinaster* (b) *Prunus avium*. $\lambda_{M,N}$: weight factor. $\nu_{M,N}$: kinetic of secondary growth factor (See equation 16 for more details).

220 that did not vary over large ranges (Table 1). Also, these coefficients do not appear to vary as a function
 221 of geometric parameters. This reflects the complexity of predicting the loading of a branch from the
 222 determinants of the main axis, and shows the importance of branching. In both cases, these variations
 223 in the λ -coefficients result in a factor 4 in the bending load between the lightly loaded and the heavily

224 loaded branches. The average values of each allometric and final geometry, indicated in table 2, will be
 225 used for the simulations.

226 Material data

227 The stress values in the normal wood were fixed according to the average maturation strains advised by
 228 Thibaut and Gril (2021). Similarly, the green wood MOE were given by the correlation between dry and
 229 green MOE identified by Thibaut and Gril (2021): $E_g = 0.89 * E_d$. Dry MOE were provided by the tropix
 230 database of CIRAD [Gérard et al. (2011)]. The density of green wood was approximated by the density of
 231 water $\rho = 1000 \text{ kg.m}^{-3}$. These inputs are summarised in Table 2.

Species	λ_M	λ_N	ν_M	ν_N	r	μ_{NW}	E_d	E_g
<i>Pinus pinaster</i>	-6.4e6	5e4	3.2	2.5	0.05	410	8.8	7.9
<i>Prunus avium</i>	-2.6e7	9.5e3	3.6	2.7	0.08	712	10.2	9.1

Table 2: Mean input characteristics of the branches. $\lambda_{N,M}$ and $\nu_{N,M}$ correspond to the allometric evolution of the normal load and bending moment, r (m) is the radius at the basal part of the branch, ν_{NW} (μ strain) is the maturation strain in the normal wood, and $E_{d,g}$ (GPa) is the dry and green modulus of the material.

233 In the following section, the case of stationary growth ($\nu_b = 0$) will be considered principally and analysed
 234 thoroughly. Situations of changing curvature will be then considered briefly.

235 Results

236 *Prunus avium*

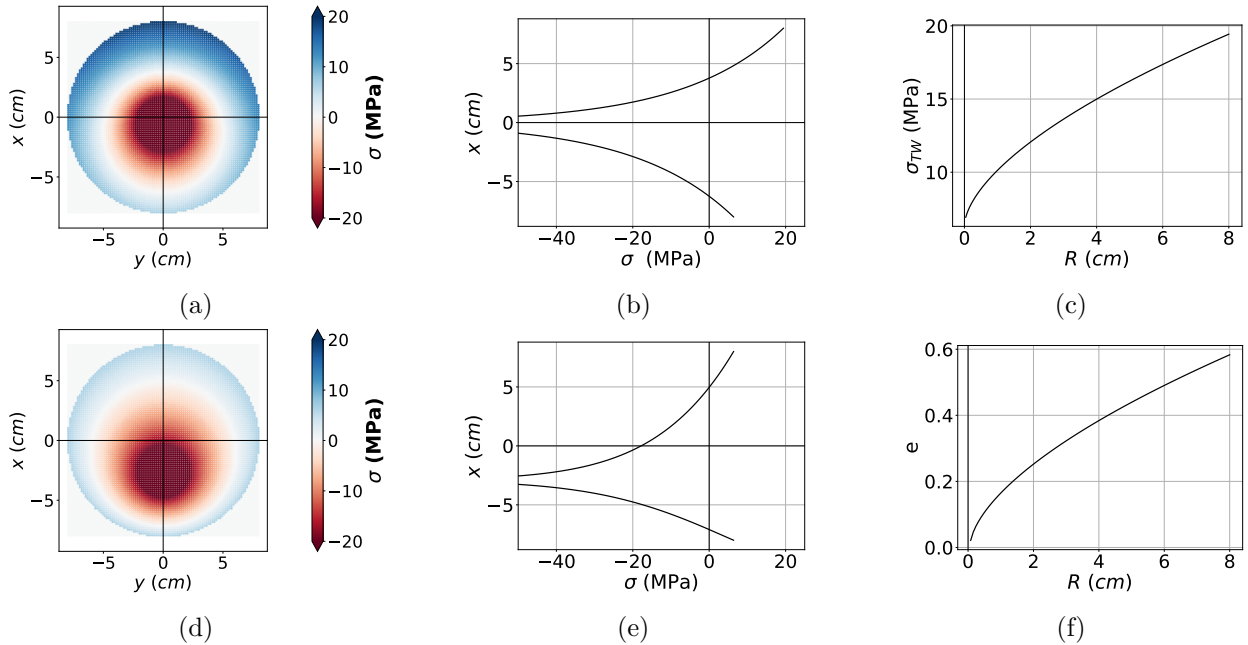
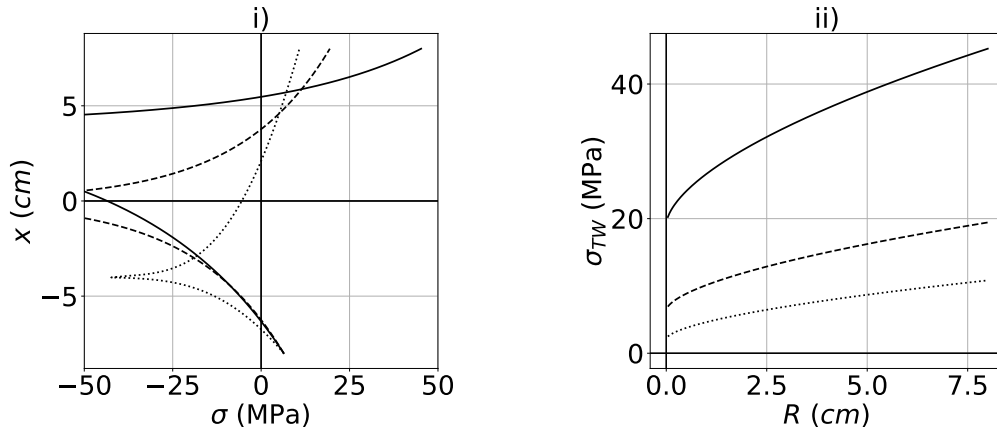


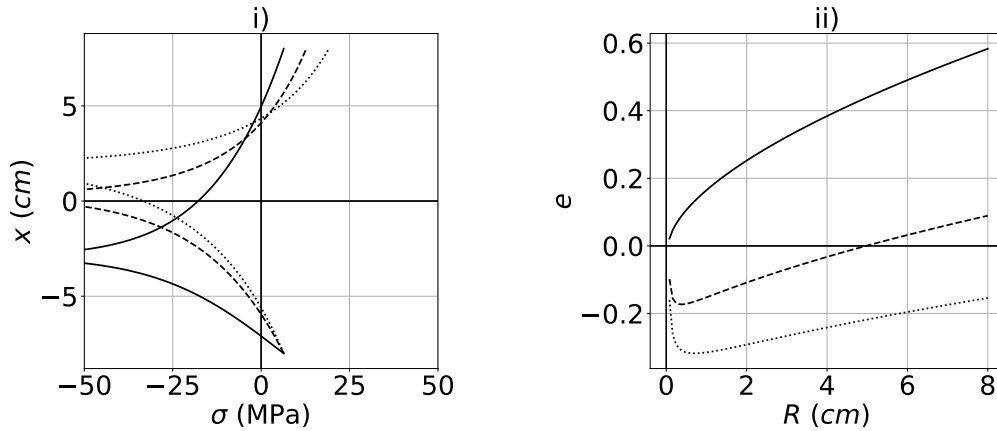
Figure 5: *Prunus avium*: the orientation of the branch is maintained by the two different processes: (a-c) the maturation stress provided by the formation of reaction wood; (d-f) the eccentric growth; (a,d) 2D visualisation of the growth stress in the whole section; (b,e) Growth stress profile on diameter $y=0$; (c,f) Parametric representation of the tropic driver, maturation stress (c) and eccentricity (f).

237 Fig 5 shows the results of the simulations for *P. avium*, when one of the factors (eccentricity or reaction
 238 wood) is set to zero. On Fig 5.a, the stress on the whole section is represented. In this case, the branch

239 maintains its orientation through the formation of reaction wood only (no eccentric growth). The area
 240 near the pith is under compression (red), while the periphery is under tension (blue), with a higher tension
 241 on the upper side, allowing to maintain the orientation. Fig 5.b shows the interpolation of the stress
 242 distribution of Fig 5.a on the main axis $y=0$. Fig 5.c represents the maturation stress in the tension wood
 243 throughout the growth of the branch. This stress becomes greater as the branch grows. The symmetric
 244 case, with no formation of reaction wood but eccentric growth, is presented in Fig 5.d-f. This example
 245 illustrates that eccentricity alone could theoretically provide the orientation control. Fig 5.f shows the
 246 evolution of the eccentricity through the radial growth of the branch. Like the reaction wood stress in the
 247 previous case, the needed eccentricity increased when the branch grew. The pattern of stress distribution of
 248 Fig 5.d is quite similar to that in in Fig 5.a , with compression near the pith and tension at the periphery,
 249 but the section is off-centred and the tension at periphery is the same all around the section, confirming
 250 the absence of reaction wood.



(a) Stress in tension wood σ_{TW} is the main driver of postural control. Different eccentricities are applied : solid line, epitrophic eccentricity $e = -0.5$, dashed line, no eccentricity, $e = 0$ and dotted line, hypotrophic eccentricity $e = 0.5$.



(b) Eccentricity e is the main driver of postural control. Different maturation gradients $\sigma_{TW} - \sigma_{NW}$ are applied : solid line, no maturation gradient ($\sigma_{TW} = \sigma_{NW}$), dashed line, $\sigma_{TW} = 2\sigma_{NW}$ and dotted line $\sigma_{TW} = 3\sigma_{NW}$.

Figure 6: Different possible options to maintain the orientation of *Prunus avium* branches: stress in reaction wood (a) or eccentricity (b). For each option, the subfigure (i) represents the total stress on diameter $y=0$, and the subfigure (ii) shows the evolution of the tropic driver (e or σ_{CW}) vs. the radius R of the branch each year.

251 Fig 6 shows the combination of the two factors. For each of them, three different scenarii were proposed. In
 252 Fig 6.a, the reaction wood controlled the orientation. Different eccentricities, ranging from -0.5 to 0.5 were

253 imposed. The resulting stress patterns are represented in Fig 6.a.i : the higher tension on the upper side
 254 maintained the posture. This tension stress becomes higher as the eccentricity becomes hypotrophic. This
 255 is confirmed by the evolution of the maturation stress induced by reaction wood through branch growth
 256 in Fig 6.a.ii. The situations where the eccentricity controlled the posture are shown in Fig. 6.b. Where
 257 uniform tension was imposed ($\sigma_{TW} = 2\sigma_{NW}$, $\sigma_{TW} = 3\sigma_{NW}$), the eccentricity pattern became particular:
 258 we observed a decrease during the first year, followed by an increase (Fig 6.b.ii). This is explained by the
 259 growth scenario: at the beginning of the development, fixing a uniform reaction wood formation tended
 260 to right-up the stem, while a stationary orientation was imposed. Therefore, the eccentricity process
 261 counteracted this righting up movement, leading to the initial decrease. As the branch grew, the effect of
 262 reaction wood decreased and the branch tended to bend forward: the eccentricity counteracted this trend,
 263 leading to the final increase. This coordination problem may probably be specific to our scenario that
 264 imposed a stationary orientation throughout the entire growth the branch, including the first stages of
 265 development.

266 *Pinus pinaster*

267 For *Pinus pinaster*, we used the same approach. The set of results is presented in Fig 7 and Fig 8. When
 268 no eccentricity was involved (Fig 7.a-c), a light compression stress was observed on the lower side of the
 269 section. When the branch grew, the compression stress increased (Fig 7.c). In case of no reaction wood
 270 formation (i.e. homogeneous maturation stress), the distributions of growth stress and eccentricity (Fig
 271 7.d-f) were quiet similar to the previous example with the birch tree: tension in periphery, compression
 272 near the pith, and an increasing eccentricity with branch growth.

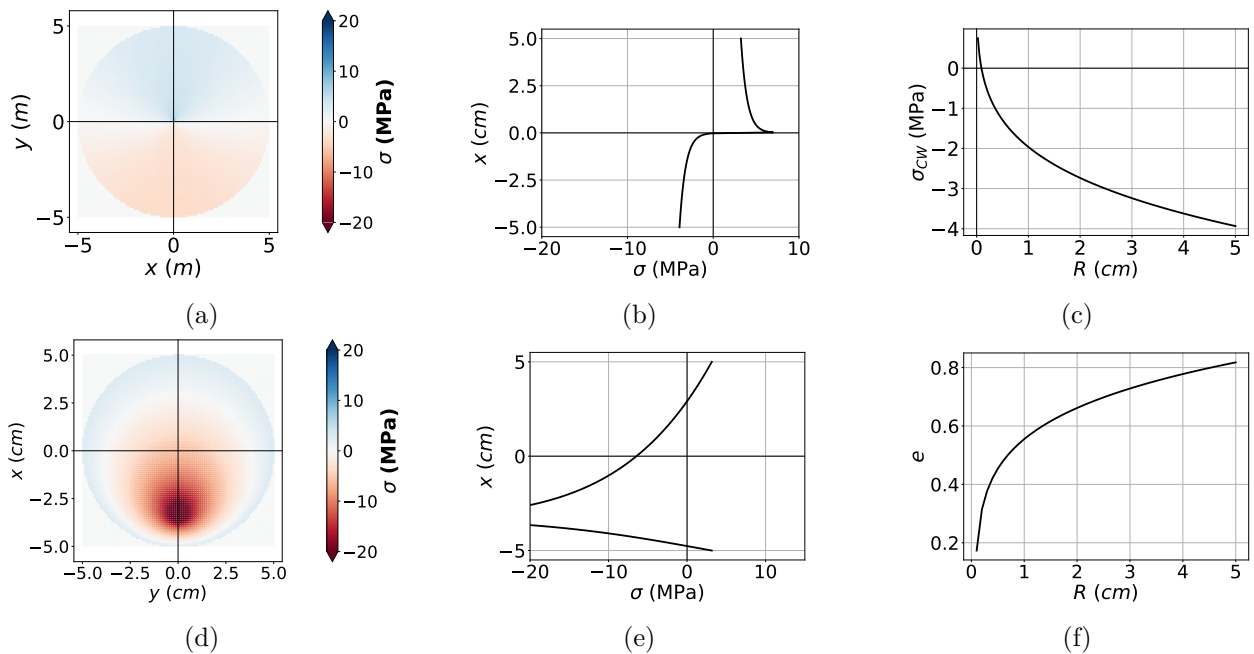
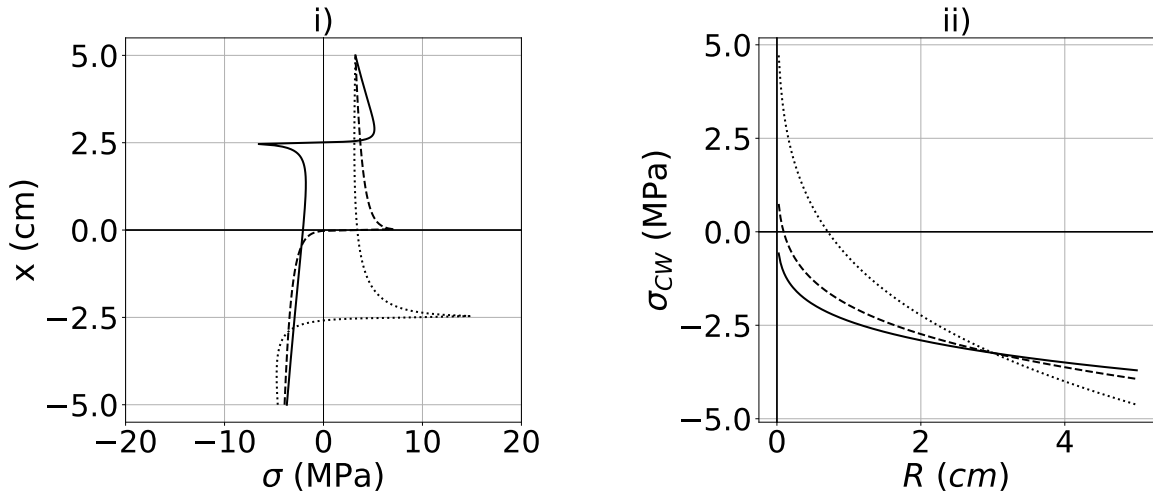


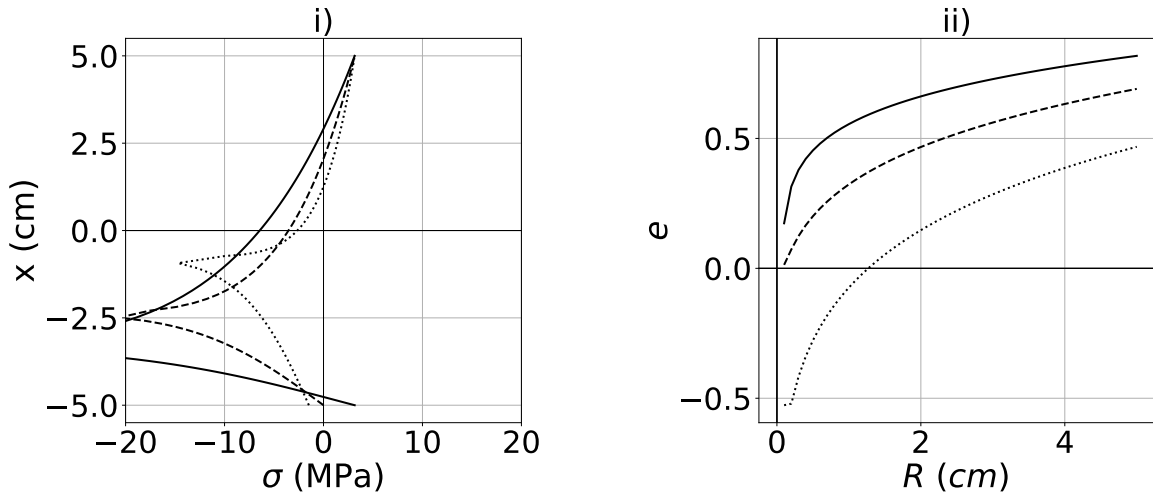
Figure 7: *Pinus pinaster*: the orientation of the branch is maintained by the two different processes: (a-c) the maturation stress provided by the formation of reaction wood; (d-f) the eccentric growth; (a,d) 2D visualisation of the growth stress in the whole section; (b,e) Growth stress profile on diameter $y=0$; (c,f) Parametric representation of the tropic driver, maturation stress (c) and eccentricity (f).

273 The combination of the two factors is shown in Fig 8. As in *Prunus avium*, different eccentricities were
 274 imposed (Fig 8.a): the more epitrophic the eccentricity, the higher reaction wood maturation stress.
 275 Although the different compression stress levels were close, the dynamic of this stress within the growth of
 276 the branch was different (Fig 8.a.ii). Also, the stress pattern exhibits a difference near the pith (Fig. 8.a.i),

277 with some tension in this area for eccentricity $e = 0.5$. In case of a uniform reaction wood maturation
 278 (8.b), the profile remained quite similar to birch tree. We could not impose a too low compression stress
 279 because of the above-mentioned coordination incompatibility.



(a) Stress in compression wood σ_{CW} is the main driver of postural control. Different eccentricities are applied : solid line, epitrophic eccentricity $e = -0.5$, dashed line, no eccentricity, $e = 0$ and dotted line, hypotrophic eccentricity $e = 0.5$.



(b) Eccentricity e is the main driver of postural control. Different constant maturation gradients $\sigma_{NW} - \sigma_{CW}$ are applied : solid line, no maturation gradient ($\sigma_{NW} = \sigma_{CW}$), dashed line, $\sigma_{CW} = 0$. Dotted line is the maximal absolute value of σ_{CW} before divergence of the computation.

Figure 8: Different possible options to maintain the orientation of *Pinus pinaster* branches: stress in reaction wood (a) or eccentricity (b). For each option, the subfigure (i) represents the total stress on the diameter $y=0$, and the subfigure (ii) shows the evolution of the tropic driver (e or σ_{CW}) vs. the radius R of the branch each year.

280 Influence of branch orientation: the stationarity hypothesis

281 In order to evaluate the relevance of the stationarity hypothesis, i.e., the branch keeps the same orientation,
 282 different growth scenarii were considered. For each branch, the case of active up-righting or passive
 283 bending was modelled (using equation 17). Passive bending was driven by increasing weight, calculated
 284 on the modelled branches. Up-righting was driven by the maturation gradient, which was set at 400

285 μ strain ($\sigma \approx 3.2$ MPa) for pine and 700 μ strain ($\sigma \approx 6.2$ MPa) for cherry (the gradient was of the order of
 286 magnitude of normal wood stress). The results are shown in Fig 9. In cherry, no major change of the stress
 287 pattern was observed. In contrast, the pattern changed greatly for pine. For a passive-bending branch, a
 288 'V' profile and the absence of compression wood were observed. For up-righting, the previously-mentioned
 289 profile with tension at the pith was observed.

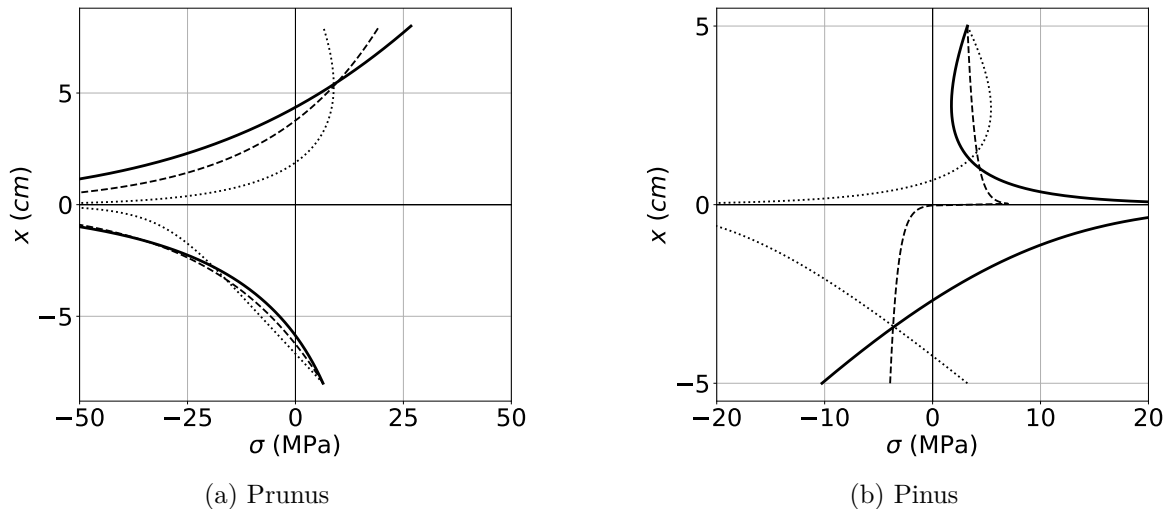


Figure 9: Distribution of growth stresses on diameter $y=0$ for different orientation scenarios. Solid line, up-righting movement; dashed line, stationarity; dotted line, passive bending.

290 Discussion

291 *Prunus avium*: heavily loaded hardwood

292 Regarding the stress distribution (Fig 5), using either eccentric growth or reaction wood formation led
 293 to realistic stress values (except near the pith, which is an intrinsic limit of our model. This specific
 294 point is discussed in section *Limits of the model*). In the case with no eccentricity, a tensile strain of
 295 $\mu_{RW} \approx 2140\mu$ strain ($\sigma_{TW} \approx 19.5$ MPa) was obtained, quite similar to literature values, for much smaller
 296 branches: on 4 cm plagiotropic branches of eight tree species, Tsai et al. (2012) reported an average
 297 strain in reaction wood of around 2100 μ strain, with some values up to $\approx 5000\mu$ strain. When combined
 298 with uniform eccentricity (Fig 6.a), it seems safer to promote the growth on the upper side: it minimises
 299 both high tensile stress and area with high compression stress. Interestingly, the worst case (hypotrophic
 300 eccentricity $e = -0,5$, more, solid line in Fig 6.a) led to levels approaching the limits, but previously
 301 observed [Huang et al. (2005); Tsai et al. (2012)]: $\mu_{RW} \approx 4970\mu$ strain ($\sigma_{TW} \approx 45.4$ MPa)).

302 In the absence of reaction wood (Fig 5.d-f), the eccentricity alone ensured the orientation. The maximal
 303 value was around 0.6, which corresponds to an average eccentricity of 0.35. Although the absolute value is
 304 realistic, average eccentric found in literature is on the opposite side. For example, Hung et al. (2017)
 305 performed measurements on 10 plagiotropic branches of *Koelreuteria elegans* (Seem.) A.C.Sm. The average
 306 radius was 2.6 cm, and the average eccentricity had an average value of -0.37, with a maximum at -0.54.
 307 Unpublished data on more than 150 branches from six different temperate species showed very different
 308 patterns, depending from the species, but eccentricity was mainly hypotrophic. These results suggest that
 309 eccentricity doesn't usually counteract gravity: its action counteracts the one of tension wood, leading to
 310 non-optimal stress patterns. An extensive measurement campaign on branches would be needed to clarify
 311 this point.

312 Also the combination of radial growth eccentricity with uniform maturation stress showed the same tendency
 313 as the dual combination (uniform eccentricity): a higher maturation stress led to a larger eccentricity.

314 Comparing all simulations, the most theoretical optimal case was a constant positive eccentricity (dotted
315 line in Fig 6.a), which is again not what is showed by experimental observations. It raises interesting
316 question on the main mechanical driver of branch construction. From a biological point a view, it could be
317 less "costly" to produce tension wood than to produce a large amount of wood for an eccentricity result.
318 But this hypothesis was never investigated. Also, more work is needed to understand how tension wood
319 and eccentricity are linked in angiosperm trees: since they may have some uncoordinated action, we can
320 wonder if they have common triggered factors.
321 Finally, these results suggest that growth eccentricity doesn't have the same role in branches and trunks:
322 Alm eras et al. (2005) showed that eccentricity in leaning stems explains $\approx 29\%$ of the of the curvature!

323 *Pinus pinaster*: lightly loaded softwood

324 First of all, the values of the stress distribution were much lower than for *Prunus avium*. This was
325 explained by the size of the modelled branches: the average bending moment is much higher for cherry
326 tree than for pine, by a factor of roughly 10 (see λ_M and λ_N in Table 2). The effect of each factor alone
327 (Fig 7) suggested that maturation is a much more efficient option than eccentricity. To ensure the same
328 growth scenario, the eccentricity alone rose to about 0.8, which is close to a theoretical limit, whereas
329 maturation alone led to low maturation strains in compression wood ($<500 \mu\text{strain}$, corresponding to 4
330 MPa). Besides, this eccentricity was not in the direction of what is commonly observed. This point remains
331 logical, because without compression wood, the epitrophic eccentricity is the only way to counteract the
332 effect of gravity.

333 A uniform eccentricity combined with reaction wood formation led to quite similar patterns (Fig 8.a):
334 for this range of loading, the eccentricity had little influence on stress distribution. Considering that the
335 density of elastic energy is proportional to the square of the stress, the pattern produced a low level of
336 stored elastic energy, possibly reducing the risk of mechanical failure. Also, although eccentricity did
337 not bring much variations in the value of the maturation stress, it considerably modified the shape of
338 the resulting stress profiles (Fig 8.a.i). Indeed, these profiles can become 'crenellated' (Fig 8.a.i, dashed
339 curve for zero eccentricity, solid curve for $e = -0.5$) or include tension at the pith (dotted line for
340 $e = 0.5$). It seems that before producing tension in the pith, an efficient configuration could be reached by
341 generating compression below the pith and tension above. Ideally, this may be a very relevant option for
342 branches. These results about the mechanical strategies of branches should be confronted to experimental
343 measurements. Otherwise, these pattern changes could also be an optimisation of the residual strength of
344 wood: compression wood is known to have high compressive strength conferred by its high lignin content
345 and cell wall structure. Generating some tension at the pith allows the branch to create more compression
346 wood. To answer this question it would be necessary to take into account strength parameters in our
347 stress computation model. Adding a damage-elastoplastic law would also allow to study the effects of
348 stress relaxation and to observe if some profiles, that are here not optimal for maintaining the branch
349 orientation, could possibly become optimal for resisting breakage.

350 Using eccentricity combined to formation (Fig 8.b) leads to usual patterns, with compression near the pith,
351 tension on the upper side and compression on the lower one. Eccentricity is epitrophic: this is the opposite
352 to what is usually observed: unpublished data on 20 branches (average radius of 3 cm) of *Pinus nigra*
353 showed an average eccentricity of -0.2. This non-intuitive result is partly explained by our hypothesis of
354 uniform stiffness, as will be discussed later. It is also explained here by the change of sign between normal
355 wood and compression wood. In the early stages of growth, as long as the stress in the compression wood is
356 lower than in the normal wood, the best option to maintain the orientation is to do epitrophic eccentricity.
357 Once the stress in the compression wood becomes higher than in the normal wood, it is more efficient to
358 do hypotrophic eccentricity. Our scenarios do not allow us to reach stress levels in compression that are
359 higher than the stress in normal wood. This is due to the above mentioned incompatibility of our scenario.

360 Influence of branch orientation : the stationary hypothesis

361 In both trees, the orders of magnitude are compatible with a mechanical safety margin for the branches.
362 Apart from modified tropisms (change of light environment, weight change by loss of part of the branch,
363 etc.), the maintenance of the orientation is quite common for real branches. However our simulations
364 suggest that if, for any reason, branches need to modify their orientation, they can do it without taking
365 too much mechanical risk.

366 Vertical bending moment vs horizontal bending and torsion moments

367 One of the hypotheses of our model was that the vertical bending moment (M_y) prevails over the torsional
368 M_z and horizontal bending M_x moments. This allowed to consider only one direction of eccentricity and
369 to avoid all the non-linear terms generated by the torsional components. We evaluated the maximum
370 values of the three moments for all modelled branches of each species for comparison purpose. The results
371 are presented in Fig 10. They show that for each species, the vertical moment displays much higher values
372 than the torsional and horizontal bending moments and validates our initial hypothesis.

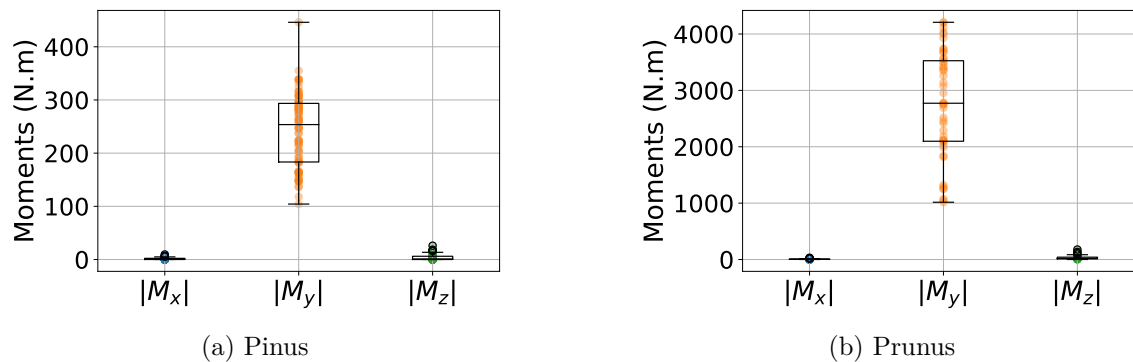


Figure 10: Comparison of maximum moments for the branches modelled in this research. M_x : horizontal moment; M_y : vertical moment; M_z : torsional moment.

373 Limits of the model

374 The hypothesis of homogeneous wood stiffness in the whole branch section is questionable. Systematic
375 stiffness differences have been observed between wood types (tension wood or compression wood vs normal
376 wood). Alm eras et al. (2005) have studied the variation of Young's modulus in the section of leaning
377 stems from 14 angiosperms and 3 gymnosperms, all coming from different families. For the angiosperms,
378 the average Young's modulus of tension wood was higher than in normal wood by 15%, while for the
379 gymnosperms, the Young's modulus was 38% lower in compression wood than in normal wood. This
380 heterogeneity of rigidity plays a role in the postural control of the stems [Alm eras et al. (2005); Huang
381 et al. (2010); Hung et al. (2017)]. In our case, either a higher rigidity in tension wood or a lower one in
382 compression wood would make the branch bend upward. In the current formulation of the model imposing
383 an homogeneous stiffness, an almost equivalent effect would have been obtained by an initial offset in the
384 eccentricity. Calling this offset tentatively 'compensating eccentricity' e_c (Fig 11), the model computed a
385 total eccentricity, e , combining e_c and the "real" eccentricity needed to maintain the orientation. Therefore,
386 in case in formation on one side, the eccentricity displayed needs to be offset by e_c to correspond to
387 more realistic situations. This explains, for instance, why the simulations for the softwood resulted in
388 hypertrophic eccentricity while it is well-known that inclined softwood stems usually exhibit hypotropic
389 eccentricity. Although data are missing to approximate the value of this parameter, and further work
390 is needed to assess theoretically the possible equivalence between rigidity variations and eccentricity,
391 the available information on relative stiffness of normal wood and suggests a more important effect in

392 gymnosperms than in angiosperms.

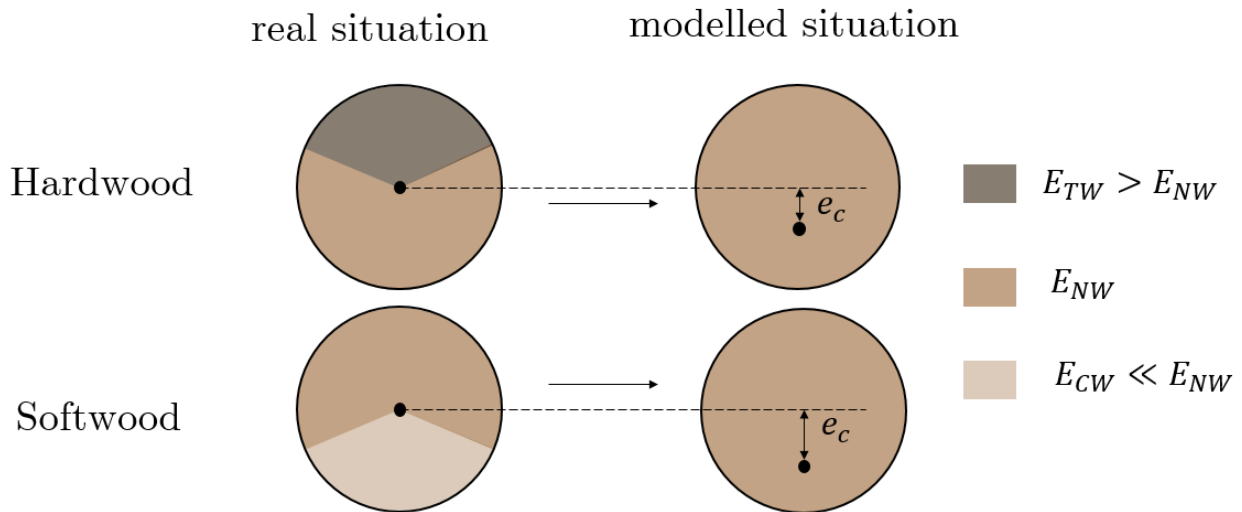


Figure 11: How the hypothesis of a uniform wood stiffness impacts the initial position of the pith. e_c : pith offset equivalent to a centered pith with heterogenous wood properties; E_{TW}, E_{NW}, E_{CW} : Longitudinal Young's modulus of tension, normal, compression wood, respectively.

393 The evaluation of the stress during the first stages of branch development is another issue of the model. In
394 almost every stress profile, a tension or compression peak is generated in the pith. It generally exceeds the
395 wood strength, which is not compatible with branch sustainability. This point could be corrected in two
396 ways. First, the role of the bark could be taken into account. Its importance in postural maintenance was
397 clearly highlighted [Clair et al. (2019); Ghislain et al. (2019)]. Our model could include the mechanical
398 action of bark in the early stages of branch development. This improvement would require additional data
399 about the mechanical behaviour of the bark but would bring more realistic stress predictions and limit
400 the artefacts at the pith. A second exciting perspective would be to take into account the elastoplastic
401 behaviour of wood. By imposing a realistic plastic strain limit, the peak at the pith would then disappear;
402 the increments would be spread over the middle part of the section, thus modifying the non-realistic
403 patterns previously observed.

404 Finally, modelling the evolution of normal force and bending moment loads by allometric laws remains
405 questionable. Indeed, the orientation of the branch may vary with time, which implies variations of the
406 effect of weight. For example, modelling a constant increase of the normal force is inappropriate if the
407 inclination of the branch decreases with time. An improvement of our model could be the construction
408 of loads based on equivalent length allometries taking into account the mass of the branch, and the
409 computation of the loads for each position in the right reference frame.

410 Conclusion and perspectives

411 A semi-analytical growth stress model has been developed in the context of branch development. This
412 model was applied to test the effectiveness of two well-known biomechanical processes of woody plants to
413 control the orientation of their axes: eccentric radial growth and formation. For the hardwood branches,
414 the computations highlighted that the eccentricity needed to maintain orientation did not corroborate the
415 observations reported in literature. This suggests that this parameter probably provides another function
416 than the orientation control, like the improved bending strength of the branch that provides it a greater
417 mechanical safety. For the softwood branches, although the model showed that eccentric radial growth
418 did not play a major role in maintaining the branch's orientation, it does modify the shape of the stress
419 profiles in the cross section of the branch. A few odd and critical profiles, crenellated or with tension near

420 the pith, have been identified. Their analysis provided exciting perspectives for further experimental works
421 to gather real data.

422 Now that a complete model is available, it becomes crucial to start experimental investigations on branches
423 in order to compare the outputs with real in situ observations. Especially, we need to evaluate the relevance
424 of the different biological processes used by branches to ensure their mechanical sustainability over the
425 years.

426 From a biological point of view, a key point for understanding branch sizing is the question of biomass
427 costs. Building additional wood on one side or forming are carbon sinks with possible trade-offs. In
428 order to investigate this point, our model could help by affecting a cost to the production of as well as to
429 eccentric growth. The resulting computations could then help to understand the relevance of some options
430 and would lead to coupling the biomechanical point of view to other biological considerations.

References

- 431
- 432 T. Alméras, D. Jullien, and J. Gril. *Modelling, Evaluation and Biomechanical Consequences of Growth Stress*
 433 *Profiles Inside Tree Stems*, pages 21–48. Springer International Publishing, Cham, 2018. ISBN 978-3-319-
 434 79099-2. doi: 10.1007/978-3-319-79099-2_2. URL https://doi.org/10.1007/978-3-319-79099-2_2.
- 435 T. Alméras and B. Clair. Critical review on the mechanisms of maturation stress generation in trees.
 436 *Journal of The Royal Society Interface*, 13(122):20160550, 2016. doi: 10.1098/rsif.2016.0550. URL
 437 <https://royalsocietypublishing.org/doi/abs/10.1098/rsif.2016.0550>.
- 438 T. Alméras and M. Fournier. Biomechanical design and long-term stability of trees: Morphological and
 439 wood traits involved in the balance between weight increase and the gravitropic reaction. *Journal of*
 440 *Theoretical Biology*, 256(3):370–381, 2009. ISSN 0022-5193. URL [http://www.sciencedirect.com/
 441 science/article/pii/S0022519308005389](http://www.sciencedirect.com/science/article/pii/S0022519308005389).
- 442 T. Alméras, A. Thibaut, and J. Gril. Effect of circumferential heterogeneity of wood maturation strain,
 443 modulus of elasticity and radial growth on the regulation of stem orientation in trees. *Trees*, 19(4):
 444 457–467, 2005. ISSN 1432-2285. URL <https://doi.org/10.1007/s00468-005-0407-6>.
- 445 P. Ancelin, T. Fourcaud, and P. Lac. Modelling the biomechanical behaviour of growing trees at the forest
 446 stand scale. part i: Development of an incremental transfer matrix method and application to simplified
 447 tree structures. *Annals of Forest Science*, 61(3):263–275, 2004.
- 448 R. R. Archer. On the distribution of tree growth stresses. ii. stresses due to asymmetric growth strains.
 449 *Wood Science and Technology*, V10:293–309, 1976.
- 450 R. R. Archer and F. E. Byrnes. On the distribution of tree growth stresses – part i: An anisotropic
 451 plane strain theory. *Wood Science and Technology*, 8(3):184–196, 1974. ISSN 1432-5225. URL
 452 <https://doi.org/10.1007/BF00352022>.
- 453 J.-F. Barczi, H. Rey, Y. Caraglio, P. de Reffye, D. Barthélémy, Q. X. Dong, and T. Fourcaud. AmapSim:
 454 A Structural Whole-plant Simulator Based on Botanical Knowledge and Designed to Host External
 455 Functional Models. *Annals of Botany*, 101(8):1125–1138, 09 2007. ISSN 0305-7364. doi: 10.1093/aob/
 456 mcm194. URL <https://doi.org/10.1093/aob/mcm194>.
- 457 D. Barthélémy, Y. Caraglio, and S. Sabatier. 4.1 crown architecture of valuable broadleaved species.
 458 *Valuable broadleaved forests in Europe*, 22:87, 2009.
- 459 D. Barthélémy and Y. Caraglio. Plant Architecture: A Dynamic, Multilevel and Comprehensive Approach
 460 to Plant Form, Structure and Ontogeny. *Annals of Botany*, 99(3):375–407, 01 2007. ISSN 0305-7364.
 461 doi: 10.1093/aob/mcl260. URL <https://doi.org/10.1093/aob/mcl260>.
- 462 Y. Caraglio. Le développement architectural du merisier. *Forêt Entreprise 107*, (107):72–80, 1996.
- 463 B. Clair, B. Ghislain, J. Prunier, R. Lehnebach, J. Beauchêne, and T. Alméras. Mechanical contribution
 464 of secondary phloem to postural control in trees: the bark side of the force. *New Phytologist*, 221(1):
 465 209–217, 2019. doi: <https://doi.org/10.1111/nph.15375>. URL [https://nph.onlinelibrary.wiley.
 466 com/doi/abs/10.1111/nph.15375](https://nph.onlinelibrary.wiley.com/doi/abs/10.1111/nph.15375).
- 467 T. Coudurier, D. Barthelemy, B. Chanson, F. Courdier, and C. Loup. Premier résultats sur la modélisation
 468 du pin maritime pinus pinaster ait.(pinaceae). *Architecture des arbres fruitiers et forestiers*, page 306,
 469 1993.
- 470 C. Coutand, M. Fournier, and B. Moulia. The gravitropic response of poplar trunks: Key roles of
 471 prestressed wood regulation and the relative kinetics of cambial growth versus wood maturation.
 472 *Plant Physiology*, 144(2):1166–1180, 2007. ISSN 0032-0889. doi: 10.1104/pp.106.088153. URL [http:
 473 //www.plantphysiol.org/content/144/2/1166](http://www.plantphysiol.org/content/144/2/1166).

- 474 J. B. Fisher and J. W. Stevenson. Occurrence of reaction wood in branches of dicotyledons and its
475 role in tree architecture. *Botanical Gazette*, 142(1):82–95, 1981. doi: 10.1086/337199. URL <https://doi.org/10.1086/337199>.
476
- 477 T. Fourcaud, F. Blaise, P. Lac, P. Castéra, and P. de Reffye. Numerical modelling of shape regulation and
478 growth stresses in trees. *Trees*, 17(1):31–39, 2003. ISSN 1432-2285. URL [https://doi.org/10.1007/
479 s00468-002-0203-5](https://doi.org/10.1007/s00468-002-0203-5).
- 480 M. Fournier, B. Chanson, D. Guitard, and B. Thibault. Mécanique de l’arbre sur pied : modélisation d’une
481 structure en croissance soumise à des chargements permanents et évolutifs. 1. analyse des contraintes de
482 support. 1991a.
- 483 M. Fournier, B. Chanson, D. Guitard, and B. Thibault. Mécanique de l’arbre sur pied : modélisation d’une
484 structure en croissance soumise à des chargements permanents et évolutifs. 2. analyse tridimensionnelle
485 des contraintes de maturation, cas du feuillu standard. 1991b.
- 486 M. Fournier, H. Baillères, and B. Chanson. Tree biomechanics : growth, cumulative prestresses, and
487 reorientations. *Biomimetics*, 2(3):229–251, 1994.
- 488 B. Ghislain, T. Alméras, J. Prunier, and B. Clair. Contributions of bark and tension wood and role of the
489 g-layer lignification in the gravitropic movements of 21 tropical tree species. *Annals of Forest Science*,
490 76(4):107, 2019. ISSN 1297-966X. URL <https://doi.org/10.1007/s13595-019-0899-7>.
- 491 J. Gérard, D. Guibal, S. Paradis, M. Vernay, J. Beauchêne, L. Brancheriau, I. Châlon, C. Daigremont,
492 P. Détienne, D. Fouquet, P. Langbour, S. Lotte, M.-F. Thévenon, C. Méjean, and A. Thibaut. Tropix 7,
493 2011. URL <http://tropix.cirad.fr/en>.
- 494 F. Hallé, R. A. Oldeman, and P. B. Tomlinson. *Tropical trees and forests: an architectural analysis*.
495 Springer Verlag, 1978.
- 496 P. Heuret, C. Meredieu, T. Coudurier, F. Courdier, and D. Barthélémy. Ontogenetic trends in the
497 morphological features of main stem annual shoots of pinus pinaster (pinaceae). *American Journal of
498 Botany*, 93(11):1577–1587, 2006. doi: <https://doi.org/10.3732/ajb.93.11.1577>. URL [https://bsapubs.
499 onlinelibrary.wiley.com/doi/abs/10.3732/ajb.93.11.1577](https://bsapubs.onlinelibrary.wiley.com/doi/abs/10.3732/ajb.93.11.1577).
- 500 Y.-S. Huang, S.-S. Chen, L.-L. Kuo-Huang, and C.-M. Lee. Growth strain in the trunk and branches of
501 chamaecyparis formosensis and its influence on tree form. *Tree Physiol*, 25(9):1119–1126, Sept. 2005.
502 ISSN 0829-318X. URL <https://doi.org/10.1093/treephys/25.9.1119>.
- 503 Y.-S. Huang, L.-F. Hung, and L.-L. Kuo-Huang. Biomechanical modeling of gravitropic response of
504 branches: roles of asymmetric periphery growth strain versus self-weight bending effect. *Trees*, 24(6):
505 1151–1161, 2010. ISSN 1432-2285. URL <https://doi.org/10.1007/s00468-010-0491-0>.
- 506 L.-F. Hung, C.-C. Tsai, S.-J. Chen, Y.-S. Huang, and L.-L. Kuo-Huang. Study of tension wood in
507 the artificially inclined seedlings of koelreuteria henryi dummer and its biomechanical function of
508 negative gravitropism. *Trees*, 30(3):609–625, 2016. ISSN 1432-2285. URL [https://doi.org/10.1007/
509 s00468-015-1304-2](https://doi.org/10.1007/s00468-015-1304-2).
- 510 L.-F. Hung, C.-C. Tsai, S.-J. Chen, Y.-S. Huang, and L.-L. Kuo-Huang. Strain distribution, growth
511 eccentricity, and tension wood distribution in the plagiotropic and orthotropic branches of koelreuteria
512 henryi dummer. *Trees*, 31(1):149–164, 2017. ISSN 1432-2285. URL [https://doi.org/10.1007/
513 s00468-016-1464-8](https://doi.org/10.1007/s00468-016-1464-8).
- 514 H. Kübler. Studien über wachstumsspannungen des holzes iii. längenänderungen bei der wärmebehandlung
515 frischen holzes. *Holz Rohst Werkst*, 17(3):77–86, 1959.

-
- 516 J. E. Nicholson. A rapid method for estimating longitudinal growth stresses in logs. *Wood Science and*
517 *Technology*, 5(1):40–48, 1971. ISSN 1432-5225. URL <https://doi.org/10.1007/BF00363119>.
- 518 B. Thibaut. Three-dimensional printing, muscles, and skeleton: mechanical functions of living wood.
519 *Journal of Experimental Botany*, 70(14):3453–3466, 04 2019. ISSN 0022-0957. doi: 10.1093/jxb/erz153.
520 URL <https://doi.org/10.1093/jxb/erz153>.
- 521 B. Thibaut and J. Gril. Tree growth forces and wood properties. *Peer Community Journal*, 1:e46, 2021. doi:
522 10.24072/pcjournal.48. URL [https://peercommunityjournal.org/articles/10.24072/pcjournal.](https://peercommunityjournal.org/articles/10.24072/pcjournal.48/)
523 48/.
- 524 C.-C. Tsai, L.-F. Hung, C.-T. Chien, S.-J. Chen, Y.-S. Huang, and L.-L. Kuo-Huang. Biomechanical
525 features of eccentric cambial growth and reaction wood formation in broadleaf tree branches. *Trees*, 26
526 (5):1585–1595, 2012. ISSN 1432-2285. URL <https://doi.org/10.1007/s00468-012-0733-4>.
- 527 Y. Wang, J. Gril, and J. Sugiyama. Variation in xylem formation of viburnum odoratissimum var. awabuki:
528 growth strain and related anatomical features of branches exhibiting unusual eccentric growth. *Tree*
529 *Physiol*, 29(5):707–713, May 2009a. ISSN 0829-318X. URL [https://doi.org/10.1093/treephys/](https://doi.org/10.1093/treephys/tpp007)
530 [tpp007](https://doi.org/10.1093/treephys/tpp007).
- 531 Y. Wang, J. Gril, and J. Sugiyama. Is the branch of viburnum odoratissimum var. awabuki reaction
532 wood? unusual eccentric growth and various distributions of growth strain. In *6th Plant Biomechanics*
533 *Conference*, pages 328–334, 2009b.
- 534 H. Yamamoto, M. Yoshida, and T. Okuyama. Growth stress controls negative gravitropism in woody
535 plant stems. *Planta*, 216(2):280–292, 2002. ISSN 1432-2048. URL [https://doi.org/10.1007/](https://doi.org/10.1007/s00425-002-0846-x)
536 [s00425-002-0846-x](https://doi.org/10.1007/s00425-002-0846-x).
- 537 J. L. Yang, H. Baillères, T. Okuyama, A. Muneri, and G. Downes. Measurement methods for longitudinal
538 surface strain in trees: a review. *Australian Forestry*, 68(1):34–43, 2005. doi: 10.1080/00049158.2005.
539 10676224. URL <https://doi.org/10.1080/00049158.2005.10676224>.
- 540 M. Yoshida and T. Okuyama. Techniques for measuring growth stress on the xylem surface using strain
541 and dial gauges. 56(5):461–467, 2002. doi: doi:10.1515/HF.2002.071. URL [https://doi.org/10.1515/](https://doi.org/10.1515/HF.2002.071)
542 [HF.2002.071](https://doi.org/10.1515/HF.2002.071).

543 **Appendix A**

544 The calculation of integrals of system (3) requires preliminary elements. The situation of two consecutive
 545 rings is represented in Fig. 12. Each position x in the geometrical reference frame is expressed with respect
 546 to the position x' in the pith reference frame according to the equation:

$$x = r \cos \theta = x' - \bar{e}R \quad (24)$$

with r the radius at time t and R the radius at the final time.

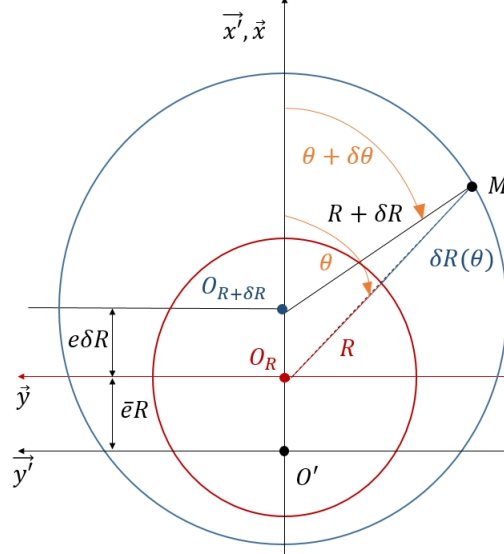


Figure 12: Representation of two consecutive rings and the elements needed to calculate $\delta R(\theta)$

547

548 The integrals of system (3) are computed as follows:

$$\begin{aligned} \int_s \delta \sigma ds &= \int_s E [\delta a + (x + \bar{e}.R)\delta b] r \delta r d\theta \\ &= E\pi R^2 (\delta a + \bar{e}.R\delta b) \\ \int_s x' \delta \sigma ds &= \int_s [\delta a + (x + \bar{e}.R)\delta b] [x + \bar{e}.R] r \delta r d\theta \\ &= E\pi R^3 \left[\bar{e}\delta a + R \left(\bar{e}^2 + \frac{1}{4} \right) \delta b \right] \end{aligned}$$

The tangential distribution of the radius increment $\delta R(\theta)$ is required to compute the maturation terms. Applying $\overrightarrow{O_R M} - \overrightarrow{O_{R+dR} M} = \overrightarrow{O_R O_{R+dR}}$ (Fig 12):

$$\begin{cases} [R + \delta R(\theta)] \cos \theta - (R + \delta R) \cos (\theta + \delta \theta) = e_R \delta R & (25a) \\ [R + \delta R(\theta)] \sin \theta - (R + \delta R) \sin (\theta + \delta \theta) = 0 & (25b) \end{cases}$$

549 By setting $\delta \theta \rightarrow 0$, it comes:

$$\begin{cases} \cos (\theta + \delta \theta) = \cos \theta - \sin \theta \delta \theta & (26a) \\ \sin (\theta + \delta \theta) = \sin \theta + \cos \theta \delta \theta & (26b) \end{cases}$$

550 Substituting (26) into (25), and combining (25a) and (25b), $\delta R(\theta)$ can finally be written as:

$$\boxed{\delta R(\theta) = \delta R [1 + e_R \cos \theta]} \quad (27)$$

Then:

$$\begin{aligned} \int_{\delta s} \sigma_0^i ds &= \int_{\delta s} \sigma_0^i(\theta) R \delta R(\theta) d\theta \\ &= \int_{\delta s} [\alpha + \beta \cos \theta] [1 + e \cos \theta] R \delta R(\theta) d\theta \\ &= \pi (2\alpha + e\beta) R \delta R \\ \int_{\delta s} x' \sigma_0^i ds &= \int_{\delta s} \sigma_0^i(\theta) (x + e.R) R \delta R(\theta) d\theta \\ &= R^2 \delta R \pi (3\alpha e + \beta e^2 + \beta) \end{aligned}$$

551 Appendix B

The matrix system (7) becomes:

$$\begin{cases} \delta a = \frac{\delta F_0 K_2 - \delta F_1 K_1}{K_0 K_2 - K_1^2} & (28a) \\ \delta b = \frac{\delta F_0 K_1 - \delta F_1 K_0}{K_1^2 - K_0 K_2} & (28b) \end{cases}$$

552 Then, numerators and denominators are calculated separately:

$$K_0 K_2 - K_1^2 = E^2 \pi^2 R^6 \left(\bar{e}^2 + \frac{1}{4} \right) - E^2 \pi^2 R^6 \bar{e}^2 = \frac{(E \pi R^3)^2}{4}$$

$$\begin{aligned} \delta F_0 K_2 - \delta F_1 K_1 &= E \pi^2 R^5 \left[-(2\alpha + e\beta) \left(\bar{e}^2 + \frac{1}{4} \right) + \bar{e} (3\alpha e + \beta e^2 + \beta) \right] \delta R + E \pi R^3 \left[R \delta N \left(\bar{e}^2 + \frac{1}{4} \right) + \bar{e} \delta M \right] \\ &= E \pi^2 R^5 \left[\alpha \left(3e\bar{e} - 2\bar{e}^2 - \frac{1}{2} \right) + \beta \left(\bar{e}e^2 - e\bar{e}^2 + \bar{e} - \frac{e}{4} \right) \right] \delta R + E \pi R^3 \left[R \delta N \left(\bar{e}^2 + \frac{1}{4} \right) + \bar{e} \delta M \right] \end{aligned}$$

$$\begin{aligned} \delta F_0 K_1 - \delta F_1 K_0 &= E \pi^2 R^4 \left[-\bar{e} (2\alpha + e\beta) + (3\alpha e + e^2 \beta + \beta) \right] \delta R + E \pi R^2 [\bar{e} R \delta N + \delta M] \\ &= E \pi^2 R^4 \left[\alpha (3e - 2\bar{e}) + \beta (1 + e^2 - e\bar{e}) \right] \delta R + E \pi R^2 [\bar{e} R \delta N + \delta M] \end{aligned}$$

Putting the calculations together, system (28) becomes:

$$\begin{cases} \delta a = \frac{4}{ER} \left[\alpha \left(3e\bar{e} - 2\bar{e}^2 - \frac{1}{2} \right) + \beta \left(\bar{e}e^2 - e\bar{e}^2 + \bar{e} - \frac{e}{4} \right) \right] \delta R + \frac{4}{E\pi R^3} \left[R \delta N \left(\bar{e}^2 + \frac{1}{4} \right) + \bar{e} \delta M \right] \\ \delta b = \frac{-4}{ER^2} \left[\alpha (3e - 2\bar{e}) + \beta (1 + e^2 - e\bar{e}) \right] \delta R + \frac{-4}{E\pi R^4} [\bar{e} R \delta N + \delta M] \end{cases}$$

553 Appendix C

554 The following calculus is based on Fig 3.b. To get the vertical bending moment M_y of unit n (eq 23), one
 555 need the calculation of each volume V_n and center of gravity G_n . Let name $D(z)$ the diametral extension
 556 of the cone. It comes:

$$V_n = \int_0^{L_n} \frac{\pi D(z)^2}{4} dz \quad (30)$$

557 where $D(z) = D_n + \left(\frac{D_{n+1}-D_n}{L_n}\right)z$. One gives

$$O_n G_n = \frac{1}{V_n} \int_0^{L_n} \frac{\pi D(z)^2}{4} z dz \quad (31)$$

Setting $\gamma = \frac{D_{n+1}-D_n}{D_n}$ and $\xi = \frac{L_n}{z}$, equations (30) and (31) become:

$$V_n = \frac{\pi D_n^2 L_n}{4} \int_0^1 (1 + \gamma \xi)^2 d\xi = \frac{\pi D_n^2 L_n}{4} \cdot \left(1 + \gamma + \frac{\gamma^2}{3}\right)$$

$$O_n G_n = \frac{1}{V_n} \frac{\pi D_n^2 L_n^2}{4} \cdot \left(\frac{1}{2} + \frac{2\gamma}{3} + \frac{\gamma^2}{4}\right)$$

558 So, finally, $O_n G_n$ can be written:

$$O_n G_n = \frac{L_n}{2} \left(\frac{1 + \frac{4}{3}\gamma + \frac{1}{2}\gamma^2}{1 + \gamma + \frac{1}{3}\gamma^2} \right) \quad (32)$$